An Efficient Dual-Time Implicit Method for High-Lift Aerodynamics Using Differential Reynolds-Stress Modelling

A. Jahangirian and L. J. Johnston***
**Amirkabir University of Technology, Aerospace Engineering Department*
Hafez Avenue, Tehran, 15875-4413, Iran
***University of Salford, School of Computing, Science and Engineering*
Salford, Greater Manchester, M5 4WT, United Kingdom

Abstract

A method to compute the aerodynamics of multi-element aerofoil, high-lift systems is outlined. The Reynolds-averaged Navier-Stokes equations are solved using an unstructured-grid approach, together with a finite-volume spatial discretisation and a dual-time implicit, time-marching solution procedure. Turbulence modelling is at the differential Reynolds stress level, in order to capture the anticipated influence of significant streamline curvature on the flow development, particularly for landing configurations. Results are presented comparing predictions with experimental data from the UK's National High-Lift Programme. In general, good agreement is obtained but further work is required to incorporate transition prediction which appears to have an influence on the stall mechanism.

1. Introduction

Mechanical high-lift system, comprising trailing-edge flaps and leading-edge slats, are used during the take-off and landing phases of flight to provide additional lifting capability at low speed beyond that of a wing's cruise configuration. The aerodynamic performance of the high-lift system has a significant impact on the overall performance of the aircraft. In particular, a small improvement in the high-lift efficiency of the wing can lead to significant gains in payload, field and climb-out performance[1,2]. However, this must be balanced against the weight and system complexity associated with the installation and operation of the high-lift system. Nield[3] and Reckzeh[4] discuss the high-lift design process, highlighting the importance of efficient computational methods which are able to provide predictions of aerodynamic performance at flight Reynolds numbers. However, the results obtained are only as good as the models of the flow physics (turbulence models) implemented and should be used with caution. Nevertheless, Computational Fluid Dynamics (CFD) methods, based on solutions of the Reynolds-average Navier-Stokes equations are nowadays used alongside wind-tunnel testing in the high-lift design process. In this way, it is possible to get much closer to an optimised high-lift configuration using CFD methods, in terms of component angles, gaps and overlaps, before having to commit to the expense of high-Reynolds number wind tunnel models for design validation. The increased simulation capability provided by CFD is enabling the high-lift design requirements to be achieved using less-complex, and therefore cheaper and lighter, flap and slat systems. However, the accurate prediction of the flow physics around maximum-lift conditions and through the stall remains a significant challenge[5]. Viscous flow phenomena such as boundary layer transition, laminar separation bubbles, turbulent wake/boundary layer mixing and even shock wave/boundary layer interaction may all be present around maximum-lift conditions and all tend to be significantly influenced by Reynolds number[6]. There is, thus, a continuing requirement for additional high-Reynolds number experimental programmes[7], involving measurements of both mean-flow and turbulence quantities, to aid understanding of these complex flows and to provide high-quality data-sets for CFD method validation and evaluation.

The development of a practical computational method for two-dimensional, low-speed, high-lift aerodynamic flows involves three main components: a procedure for generating suitable computational grids around the multi-element aerofoil section, the implementation of a turbulence model to predict the flow physics and an efficient solution algorithm for the mean-flow and turbulence transport equations. The majority of the methods reviewed by Rumsey and Ying[5] are based on a structured-grid formulation and employ one- or two-equation turbulence models which adopt the turbulent-viscosity approach to modelling the Reynolds stresses appearing in the mean-flow equations. Using structured grids, it is relatively straightforward to generate the highly-stretched computational cells

immediately adjacent to the aerofoil surfaces which are required to resolve the boundary-layer regions in these high-Reynolds number flows. However, the turbulent boundary-layer and wake regions developing around a high-lift system can change significantly in position and thickness as the aerofoil section is pitched from small incidence angles up to and beyond the stall condition. In this situation, an unstructured-grid approach, together with flow-adaptation, may be a more efficient approach[8]. Also around maximum-lift conditions, there is significant stream-wise curvature of the turbulent wakes flowing from upstream aerofoil elements over the upper surfaces of the downstream elements. The various Reynolds normal- and shear-stress components respond in different ways to the influence of flow curvature, but this vector-like behaviour cannot be simulated using a scalar turbulent-viscosity coefficient. It is for this reason that a Reynolds-stress transport equation model is adopted in the present computational method.

2. Computational Method

2.1 Grid Generation

The unstructured grid-generation procedure used is described in detail by Marques and Johnston[9] and consists of three distinct stages. Firstly, structured-like grids, consisting of directly-triangulated quadrilateral cells, are wrapped locally around the various aerofoil surfaces and extended downstream of the trailing edges. These anisotropic-grid cells encompass all the anticipated boundary-layer and wakes regions of the flow domain. Any overlapping cells in these regions are deleted, with the quad-tree search algorithm of Löhner[10] being used to facilitate this process. Figure 1 shows views of the anisotropic-grid regions around the flap elements of the NHLP L1/T8 5-element high-lift aerofoil configuration, before and after deletion of overlapping cells.

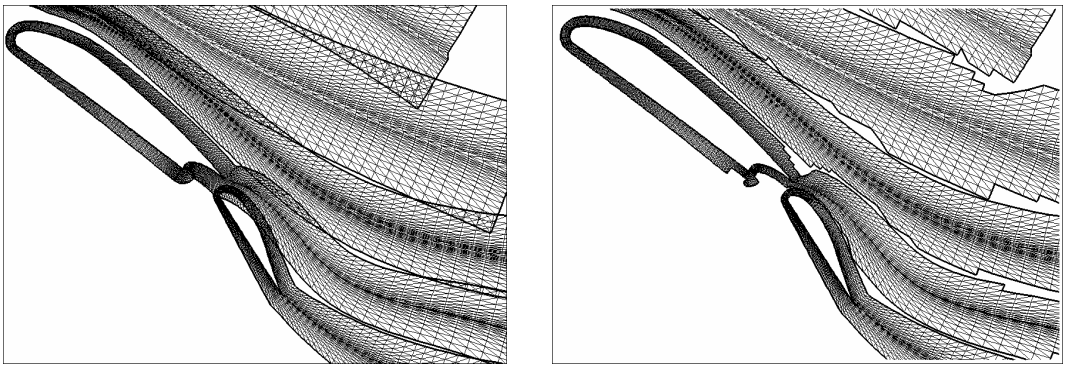

Figure 1: Anisotropic Grid Before and After Deletion of Overlapping Cells

With the anisotropic-grid regions created, the next stage in the present grid-generation method is to create an initial triangulation for the remaining part of the flow domain. This is achieved by connecting all outer-edge points of the anisotropic regions to the outer boundaries of the domain, using the Tanemura-Merrian Delaunay algorithm, as described by Mavriplis[11]. The Delaunay algorithm provides a valid initial triangulation of the inviscid-flow region, producing computational cells which are as isotropic as possible, see Figure 2.

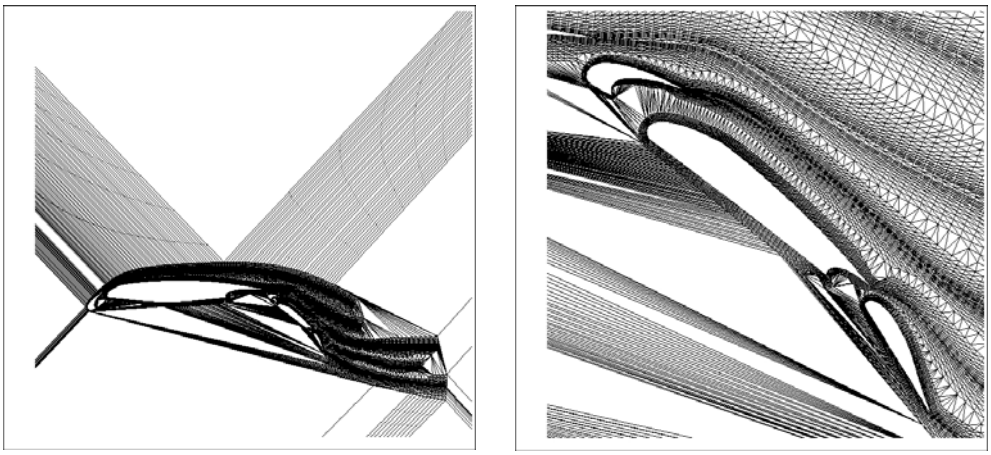

Figure 2: Initial Isotropic Grid Generation

The final stage of the grid-generation process involves refinement of the isotropic-grid regions using the cell sub-division technique of Jahangirian and Johnston[8]. The various cell-edges in the isotropic region of the grid are listed in order of their length. Each edge is then checked against desired edge-length criteria, with edges being tagged for sub-division if they fail to meet the criteria. Cell sub-division is made by splitting the longest edge, thus dividing the two cells for which the tagged edge is common. If the adjacent cells do not share the same longest edge, the neighbouring cell is sub-divided first. A Laplacian smoother is applied to the isotropic-grid regions and the outer layers of the anisotropic-grid regions, and this quality-improvement process is complemented by an edge-swapping operation. The desired grid density and quality is generally achieved after 20 iterations of the cell sub-division procedure. In contrast to most existing unstructured-grid methods, the present approach generates new cells, grid-points and the respective connectivities simultaneously. Figure 3(a) to (c) shows the inner regions of grids generated for the three NHLP high-lift configuations to be considered in the results section below.

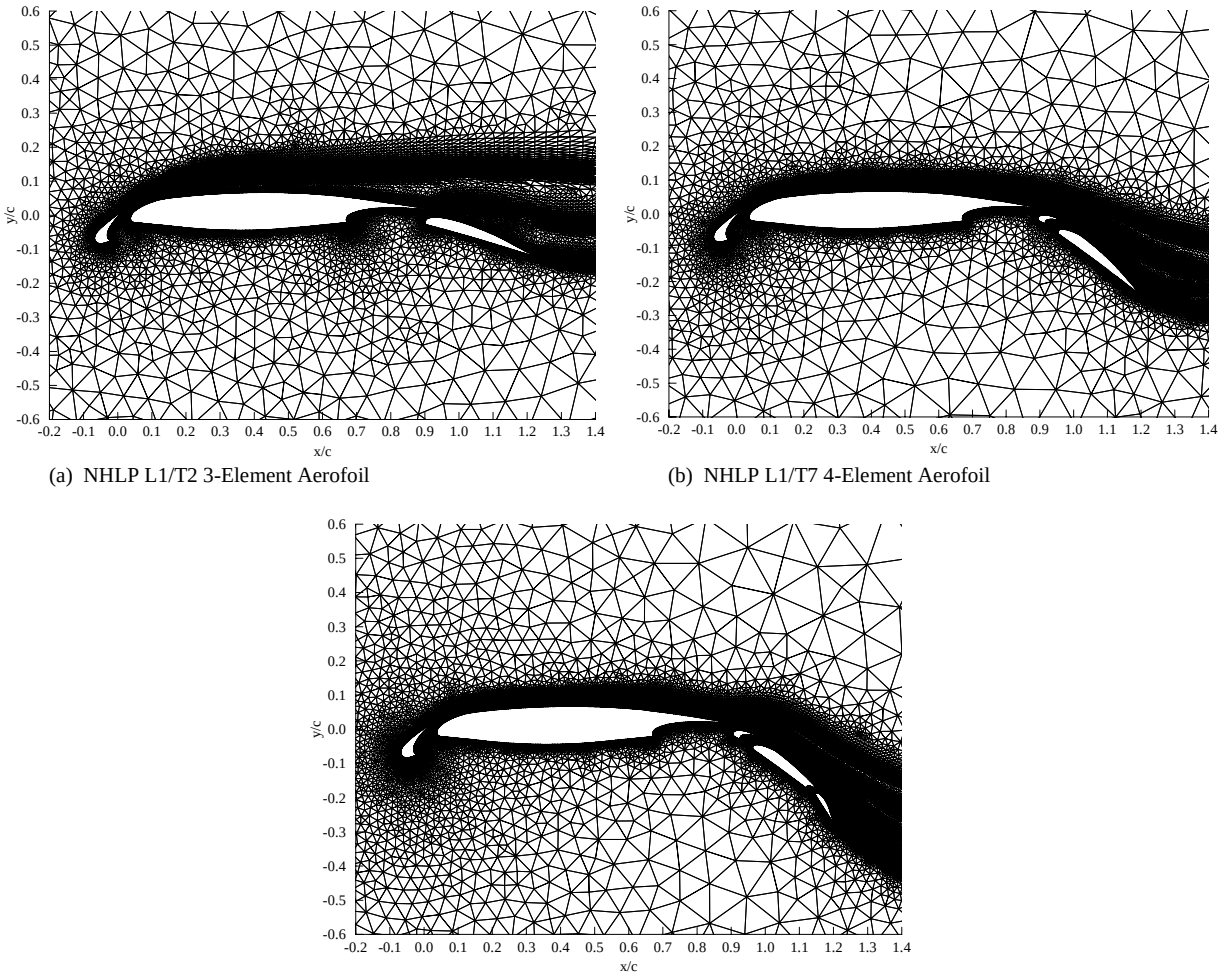

(a) NHLP L1/T2 3-Element Aerofoil

(b) NHLP L1/T7 4-Element Aerofoil

(c) NHLP L1/T8 5-Element Aerofoil

Figure 3: Computational Grids for the Three NHLP High-Lift Configurations

2.2 Governing Flow Equations

The present computational method is based on solution of the Reynolds-averaged Navier-Stokes equations applicable to two-dimensional, compressible, turbulent flow. Although the free-stream Mach numbers are of the order of 0.2 at take-off and landing conditions, there can be significant compressibility effects present, particularly around the upper surface of any leading-edge slat element. This is the reason for employing a compressible-flow solver. Also, the time-dependent, integral form of the equations is used, with steady-state solutions being obtained by time-marching procedures. The Reynolds-stress terms appearing in the governing mean-flow equations are modelled using either the turbulent-viscosity based, two-equation k-ε model of Launder and Spalding or the simplified version of the differential Reynolds-stress model (DRSM) of Launder, Reece and Rodi. This latter model solves transport equations for the three Reynolds normal-stress components, the Reynolds shear stress and the rate-of-dissipation of turbulent

kinetic energy. Further details concerning the mean-flow equations and the implementation of the *k-ε* turbulence model can be found in Johnston and Stolcis[12], with Cantariti and Johnston[13] providing the corresponding details for the DRSM turbulence model. Both models can be used with either wall-function boundary conditions or a one-equation, low-Reynolds number formulation for the near-wall regions of the flow.

2.3 Solution Algorithm

The mean-flow and turbulence-transport equations are discretised in space using the cell-centred, finite-volume formulation of Jameson *et al*[14], which employs additional numerical dissipation terms in order to facilitate smooth solutions. The resulting set of semi-discrete equations can be written as follows :

$$\frac{d(h_i\, q_i)}{dt} + R(q_i) - D(q_i) = 0 \qquad \textbf{(1)}$$

q_i is the vector of dependent variables, R_i is the residual containing the convective, diffusive and source terms, D_i contains the numerical dissipation terms and h_i is the area of computational cell i. The dual-time, implicit method of Jameson[15] is used to time-march the semi-discrete equations to a steady-state solution, as described by Jahangirian and Hadidoolabi[16] for the present unstructured-grid methodology. The time-derivative is approximated by a second-order accurate, implicit, finite-difference operator:

$$\frac{h_i}{2\Delta t}\left(3q_i^{n+1} - 4q_i^{n} + q_i^{n-1}\right) + R(q_i^{n+1}) - D(q_i^{n+1}) = 0 \qquad \textbf{(2)}$$

where n denotes a time level. It is convenient at this stage to define a new residual R^*:

$$R^*(q_i^{n+1}) = \frac{h_i}{2\Delta t}\left(3q_i^{n+1} - 4q_i^{n} + q_i^{n-1}\right) + R(q_i^{n+1}) - D(q_i^{n+1}) \qquad \textbf{(3)}$$

The solution of the steady-state problem:

$$R^*(q_i^{n+1}) = 0 \qquad \textbf{(4)}$$

is also a solution of the original set of discretised mean-flow and modelled turbulence-transport equations. Equation (4) is solved by introducing a fictitious pseudo-time τ, and setting-up a new time-dependent problem:

$$\frac{d(h_i\, q_i^{n+1})}{d\tau} + R^*(q_i^{n+1}) = 0 \qquad \textbf{(5)}$$

An explicit, four-stage scheme is used to time-march this equation to a steady-state solution, with local time-stepping and implicit residual smoothing techniques being employed to enhance the rate of convergence. Note that convergence of the pseudo time-dependent problem, equation (5), results also in convergence of the original time-dependent problem, equation (1), in real time. The dual-time, implicit approach is computationally much more efficient than a purely explicit solution procedure.

3. Results

Predictions using the present computational method are compared with experimental results from the UK's National High Lift Programme (NHLP) of the 1970's. Three different high-lift, multi-element aerofoil configurations are considered, all based on the same clean aerofoil geometry. The experimental data is described by Moir[17], and a detailed overview of the NHLP can be found in Woodward and Lean[18]. The wall-function approach to near-wall boundary conditions for the turbulence-transport equations has been employed in all cases.

3.1 NHLP L1/T2 3-Element Aerofoil Configuration

The NHLP L1/T2 3-element aerofoil section consists of a leading-edge slat and a single-slotted trailing-edge flap, and is representative of a typical take-off configuration. The flow conditions consist of a free-stream Mach number of 0.197 and a Reynolds number of 3.52 x 10^6. The DRSM turbulence model is used for the computations, with fixed transition positions assumed on the upper and lower surfaces of all aerofoil elements. The computational grid, Figure 3(a), consists of 38148 cells, 57561 cell-edges and 22742 vertices. There are 142, 280 and 203 cell-edges on the surfaces of the flap, main-aerofoil and slat elements, respectively. Computed surface pressure distributions at an incidence angle of 20.18^o are in good agreement with experiment, Figure 4. Note that sonic-flow conditions are reached on the upper surface of the leading-edge slat despite the relatively modest free-stream Mach number. Predicted and experimental variations in lift and pitching-moment coefficients with incidence angle are shown in Figure 5. Both coefficients are well-predicted up to the experimental stall angle, but the computations do not capture the observed stall behaviour. This is attributed to inadequacies in dealing with the boundary-layer transition process and the possible appearance of laminar separation bubbles on the upper surfaces of some aerofoil elements.

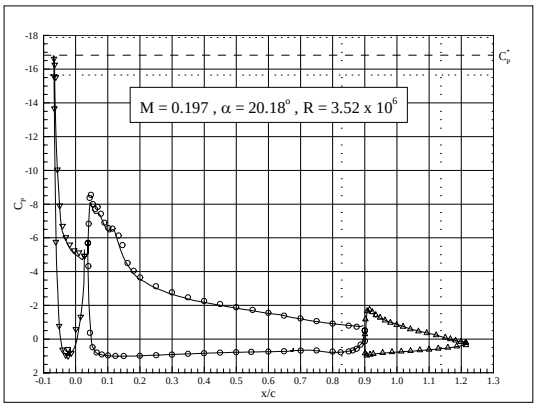

Figure 4: Surface Pressure Distribution for NHLP L1/T2 3-Element Aerofoil Section

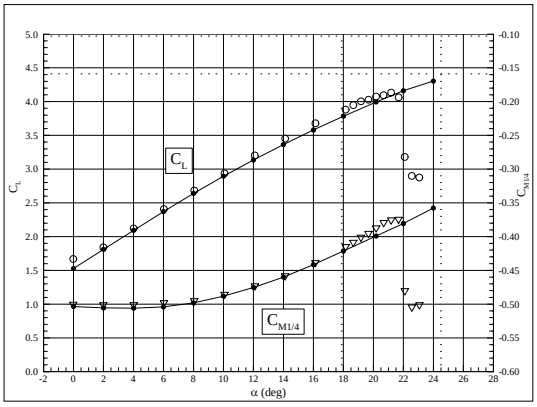

Figure 5: Lift and Pitching-Moment Coefficients for NHLP L1/T2 3-Element Aerofoil Section

3.2 NHLP L1/T7 4-Element Aerofoil Configuration

This 4-element aerofoil configuration is representative of a landing configuration and is considerably more challenging than the previous case. The influence of significant streamline curvature can be anticipated since the flap is deflected 40^o and, in the trailing-edge region, there are several wake/boundary-layer and wake/wake interactions present. The flow conditions are a free-stream Mach number of 0.161, a corrected incidence angle of 19.15^o and a Reynolds number of 2.88 x 10^6. The computational grid, Figure 3(b), consists of 48309 cells, 72898 cell-edges and 26974 vertices. There are 140, 155, 319 and 190 cell-edges on the surfaces of the flap, vane, main-aerofoil and slat elements, respectively. The results for two separate computations, comparing the performance of the *k-ε* and DRSM turbulence models, are presented. Again, fixed transition positions are assumed on the upper and lower surfaces of all

aerofoil elements. Figure 6 indicates a reasonable level of agreement between predictions and experiment for the surface pressure distributions. However, there are under-predictions of the suction levels on the upper surfaces of the vane and flap elements, Figure 7. Note also that the two turbulence models are predicting differing extents of upper-surface flow separation on the flap element, with the DRSM model giving closer agreement with experiment. The predicted iso-Mach number contours, Figure 8, show that compared to the *k-ε* model, the DRSM model predicts a much smaller recirculation at the flap trailing edge.

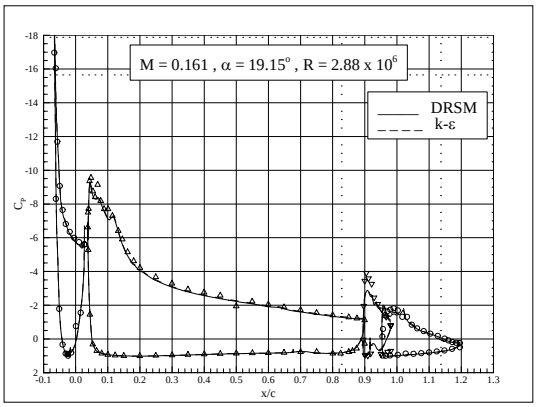

Figure 6: Surface Pressure Distribution for NHLP L1/T7 4-Element Aerofoil Section

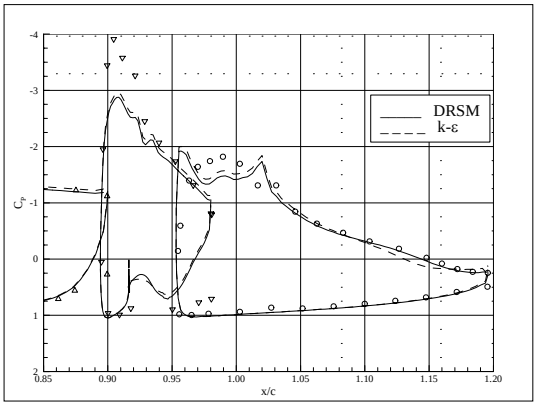

Figure 7: Vane and Flap Surface Pressures for NHLP L1/T7 4-Element Aerofoil Section

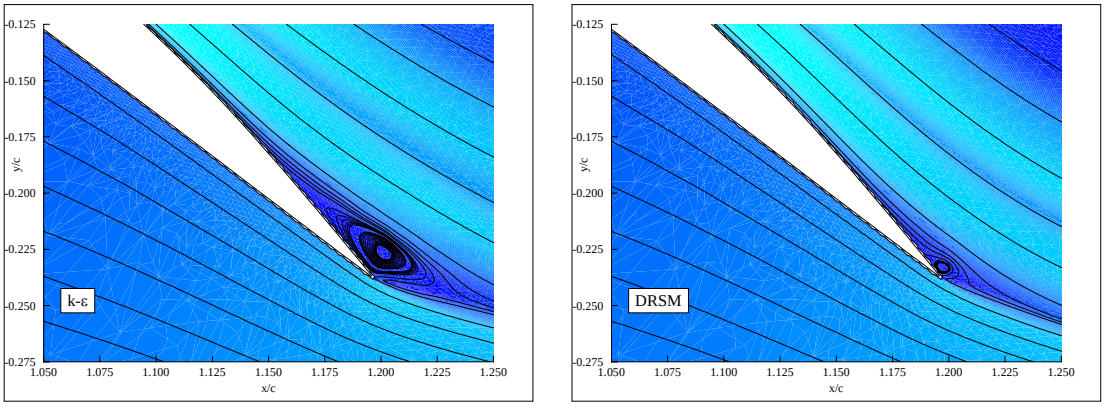

Figure 8: Iso-Mach Number Contours for NHLP L1/T7 4-Element Aerofoil Section

3.3 NHLP L1/T8 5-Element Aerofoil Configuration

The flow conditions for the 5-element aerofoil configuration are a free-stream Mach number of 0.161, a corrected incidence angle of 17.1^o and a Reynolds number of 2.88 x 10^6. The computational grid, Figure 3(c), consists of 70518 cells, 106401 cell-edges and 40152 vertices. There are 130, 264, 180, 379 and 231 cell-edges on the surfaces of the auxiliary flap, flap, vane, main-aerofoil and slat elements, respectively. The DRSM turbulence model is used for the computations, with fixed transition positions assumed on the upper and lower surfaces of all aerofoil elements. Figure 9 shows a reasonable level of agreement between predicted and experimental surface pressure distributions, although there is an under-prediction of suctions levels on the upper surfaces of all the aerofoil elements.

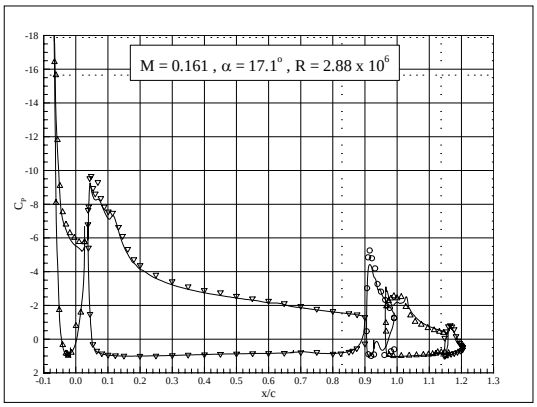

Figure 9: Surface Pressure Distribution for NHLP L1/T8 5-Element Aerofoil Section

The convergence history of the computation for the NHLP L1/T8 5-element aerofoil case, Figure 10, is typical for all of the computations presented here. The flow solutions have all been run on a Laptop PC with a 2GHz Intel Core 2 CPU and 1.24GB of RAM.

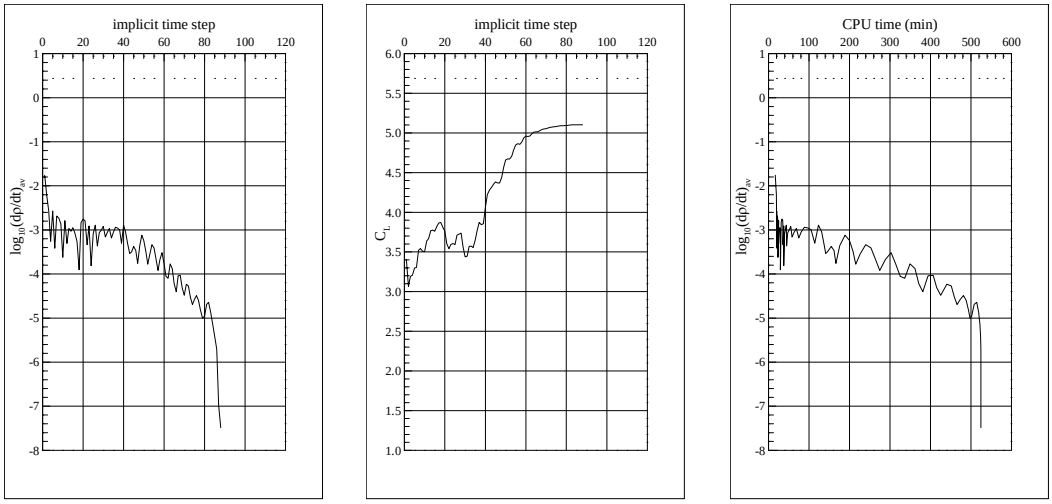

Figure 10: Convergence of Density Residual and Lift Coefficient for NHLP L1/T8 5-Element Aerofoil Section

4. Conclusions

A computational method to predict multi-element aerofoil, high-lift aerodynamics is described, with a particular emphasis on the dual-time, implicit solution procedure adopted to time-march the governing mean-flow and turbulence-transport equations to steady-state solutions. Sample results are presented, comparing predictions with experiment, for three high-lift configurations taken from the UK's National High Lift Programme (NHLP).

Encouraging levels of agreement with experimental data are obtained, which indicate the computational efficiency of the present method. The initial results do, however, point to some weaknesses in the physical modelling of these complex flows, as embodied in the turbulence models. Two particular areas for further study are the influence of the boundary-layer transition positions on the stall characteristics of the high-lift system and the incorporation of a procedure to deal with the presence of laminar separation bubbles on the upper surfaces of some aerofoil elements. Accurate drag prediction for multi-element aerofoil sections, not considered here, also remains an area of concern.

Acknowledgement

The authors would like to acknowledge the important contribution made by Simao Marques in generating the computational grids used in the present study.

References

[1] Smith, A.M.O., 'High Lift Aerodynamics', *Journal of Aircraft*, Vol.12, No.6, June 1975.
[2] Meredith, P.T., 'Viscous Phenomena Affecting High-Lift Systems and Suggestions for Future CFD Development', *High-Lift System Aerodynamics, AGARD CP-515*, Sept. 1993, pp.19-1/19-8.
[3] Nield, B.N., 'An Overview of the Boeing 777 High Lift Aerodynamic Design', *Aeronautical Journal*, Nov. 1995, pp. 361-371.
[4] Reckzeh, D., 'Aerodynamic Design of the High-Lift Wing for a Megaliner Aircraft', *Aerospace Science and Technology*, No.7, 2003, pp.107-119.
[5] Rumsey, C. and Ying, S., 'Prediction of High Lift: Review of Present CFD Capability', *Progress in Aerospace Sciences*, 38, 2002, pp.145-180.
[6] van Dam, C.P., 'The Aerodynamic Design of Multi-Element High-Lift Systems for Transport Airplanes', *Progress in Aerospace Sciences*, 38, 2002.
[7] Morgan, H., 'Experimental Test Results of Energy Efficient Transport (EET) High-Lift Airfoil in Langley Low-Turbulence Pressure Tunnel', *NASA TM-2002-211780*, 2002.
[8] Jahangirian, A. and Johnston, L.J., 'Calculation of High-Lift Aerodynamics on Adaptive Unstructured Grids', *in Proceedings of the 20th ICAS Congress* (2), pp.193-217, 1996.
[9] Marques, S.P. and Johnston, L.J., 'Unstructured Grid Generation Method and Flow Solutions for Two-Dimensional, High-Lift Aerofoil Configurations', AIAA Paper 2007-1299, *45th AIAA Aerospace Sciences Meeting and Exhibit*, 8-11 January 2007, Reno, Nevada, USA.
[10] Löhner, R., 'Finite Element Methods in CFD: Grid Generation, Adaptivity and Parallelization', *Special Course on Unstructured Grid Generation Methods for Advection Flows, AGARD AR-787* (1992).
[11] Mavriplis, D.J., 'Unstructured Mesh Generation and Adaptivity', *Algorithm and Data Structures for Structured and Unstructured Grid Generation, VKI,* 1998.
[12] Johnston, L.J. and Stolcis, 'Prediction of the High-Lift Performance of Multi-Element Aerofoils Using an Unstructured Navier-Stokes Solver', *High-Lift System Aerodynamics, AGARD CP-515*, Sept. 1993, pp.13-1/13-18.
[13] Cantariti. F.J.-J. and Johnston, L.J., 'High-Lift Navier-Stokes Computations on Unstructured Grids Using a Differential Reynolds Stress Model', *Numerical Methods for Fluid Dynamics V*, Edited by K.W. Morton and M.J. Baines, Oxford Science Publications, 1995, pp.319/325.
[14] Jameson, A., Baker, T.J. and Weatherill, N.P., 'Calculation of Inviscid Transonic Flow over a Complete Aircraft', AIAA Paper 86-0103, 1986.
[15] Jameson, A., 'Time Dependent Calculations Using Multigrid with Applications to Unsteady Flows Past Airfoils and Wings', AIAA Paper 91-1596, 1991.
[16] Jahangirian, A. and Hadidoolabi, M., 'An Implicit Solution of the Unsteady Navier-Stokes Equations on Unstructured Moving Grids', *in Proceedings of the 24th ICAS Congress* (2), 2004.
[17] Moir, I.R., 'Measurements on a Two-Dimensional Aerofoil with High-Lift Devices', *A Selection of Experimental Test Cases for Validation of CFD Codes, AGARD AR-303, A2,* 1992.
[18] Woodward, D.S. and Lean, D.E., 'Where is High-Lift Today? - A Review of Past U.K. Research Programmes', *High-Lift Systems Aerodynamics, AGARD CP-515*, Sept. 1993, pp.1-1/1-45.